Electronic and optical properties of pentagonal B$_2$C monolayer: A first-principles calculation

MOSAYEB NASERI*

Department of Physics, Kermanshah Branch, Islamic Azad University, Kermanshah, Iran
m.naseri@iauksh.ac.ir

JAFAR JALILIAN

Young Researchers and Elite Club, Kermanshah Branch, Islamic Azad University, Kermanshah, Iran.

A.H. RESHAK

New Technologies - Research Centre, University of West Bohemia, Univerzitni 8, 306 14 Pilsen, Czech Republic
School of Material Engineering, University Malaysia Perlis, 01007 Kangar, Perlis, Malaysia

The electronic and optical properties of pentagonal B$_2$C monolayer are investigated by means of the first principles calculations in the framework of the density functional theory. The cohesive energy consideration confirmers the good stability of the B2C nanostructure in this phase. The electronic band structure reveal that the valence band maximum (VBM) is located at X point of the first Brillouin zone (BZ) whereas the conduction band minimum (CBM) is situated at the center of the BZ, resulting in an indirect energy band gap of about 1.5 eV. Furthermore, a calculated low absorption and low reflection of the material in low energy ranges denotes the transparency of the B$_2$C monolayer in investigated range for normal light incidence. The obtained results may find application in fabrication of future opto-electronic devices.

Keywords: Density functional theory; Boron Carbide; Electronic properties; Optical properties.

---

*Corresponding author email address: m.naseri@iauksh.ac.ir

1. Introduction

In the past decade a variety of semiconductors, two-dimensional nanomaterials such as metal-organic frameworks (MOFs)[1,2], covalent-organic frameworks (COFs)[3], polymers[4,5,6],black phosphorus (BP)[7], silicene[8], zinc oxide[9,10] and MXenes[11]have been considered by theoretical and experimental research groups. Parallel to these studies, in recent years, a series of graphene-like materials such as silicon carbide [12], boron carbide [13], boron nitride [14,15], and beryllium carbide [16] have been predicted.

Up to now, a number of two-dimensional nanostructures of B_2C compound are predicted and investigated. A two-dimensional B_2C was predicted by the first principles calculations where the boron and carbon atoms are packed into a mosaic of hexagons and rhombuses while each carbon atom is bonded with four boron atoms, forming a planar-tetracoordinate carbon (ptC) moiety[17]. In 2012, using the density functional theory the electronic and the linear optical properties of a B_2C monolayer was studied by Shahrokhi et al. [18]. They predicted a metallic behavior for the considered B_2C structure. Recently, Li et al., predicted a new two-dimensional pentagonal B_2C sheet (penta-B_2C), with semiconducting behavior in which each pentagon contains three boron and two carbon atoms. The C atom is four-coordinated with four B atoms, and all the B atoms are three-coordinated with two C atoms and one B atom, forming a buckled 2D network [19].

In this study, to investigate the potential applications of the designed pentagonal B_2C nanosheet, the electronic and optical properties have been studied using density functional theory. The optical interband transitions, reflectivity, and optical absorption spectra are investigated to gain a good view point of optical behavior of this semiconductor nanostructure.

2. Computational details

The electronic and optical properties of pentagonal B_2C monolayer have been studied by the first principles calculations by means of the the density functional theory as implemented by the WIEN2k code [20]. The full potential linear augmented plane waves plus local orbital (FPLAPW+lo) is applied to expand the Kohn-Sham wave functions. The exchange-correlation term is produced by utilizing the generalized gradient approximation presented by Perdew-Burke-Ernzerhof (GGA-PBE) [21]. Based on Monkhorst-Pack approximation [22], $12\times12\times2$ and $30\times30\times5$ k-mesh have been considered in the whole first Brillouin zone for electronic and optical calculations, respectively. The computational input parameters are $R_{MT}K_{max}$=7, G_{max}=14 $Ry^{1/2}$ and $l_{max} = 10$. 20 Å vacuum space in the non-periodic directions (z direction) have been used to avoid two neighboring image interactions. To gain the imaginary part and the real part of the complex dielectric function, the calculation of the optical properties have been performed by using the random phase approximation (RPA) method [23] and the Kramers-Kronig relations respectively.
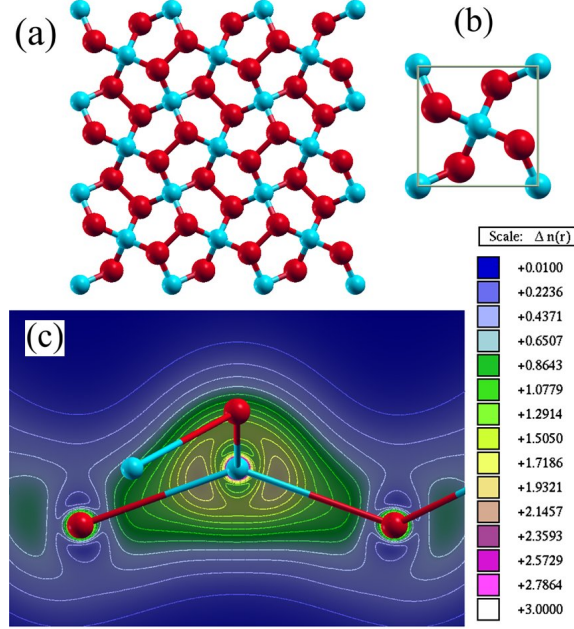
Fig. 1.   (a)A B_2C monolayer. (b)A cubic unit cell of a B_2C monolayer. (c)A two-dimensional charge distribution in B-C bond plane, the red and blue balls illustrate Boron and Carbon atoms respectively.

2.1. *Structural properties*

The lattice constants of cubic unit cell of the monolayer B2C (see Fig.1a, Fig.1b) is optimized using the thermodynamical equation state of Brich-Murnaghun [24]:

$$E(V) = E_0 + \frac{9B_0V_0}{16}\left\{\left[\left(\frac{V_0}{V}\right)^{2/3} - 1\right]^3 B_0^{'}\right\} \tag{1}$$

$$+\frac{9B_0V_0}{16}\left\{\left[\left(\frac{V_0}{V}\right)^{2/3} - 1\right]^2 \left[6 - 4\left(\frac{V_0}{V}\right)^{2/3}\right]\right\}$$

where V_0 is the initial considered volume volume, V is the deformed volume, B_0 is the bulk modulus, and $B_0^{'}$ is the derivative of the bulk modulus with respect to pressure. The obtained optimized lattice constants is 3.93 $\mathring{A}$ which show a good agreement with that obtained by Li et al. [19]. The considered unit cell contains four boron and two carbon atoms as each carbon atom is shared by four boron atoms while each boron atom is bounded with two carbon atoms and one Boron. Carbon and boron atoms in this structure form a buckled pentagonal B-C-B sandwich tri-layer network, i.e., every two neighboring B atoms in B_2C monolayer are buckled into two different atomic planes above and below the C atomic plane, respectively. After the force relaxation process to achieve most stable configuration, the calcu-

4   *M. Naseri, et al.,*

lated B-C and B-B bond lengths are about 1.58 and 1.72 $\mathring{A}$ which exhibit good agreement with that obtained by Li et al.[19].

To ensure the structural stability of B_2C monolayer, the cohesive energy is calculated. According to the definition of cohesive energy:

$$E_{coh} = \frac{E_{B_2C}^{total} - mE_B^{isolated} - nE_C^{isolated}}{m+n} \tag{2}$$

where $E_{B_2C}^{total}$, $E_B^{isolated}$ and $E_C^{isolated}$ are total energy of B_2C unit cell, energy of isolated boron and isolated carbon atoms, respectively. Also, m and n indexes refer to the number of boron and carbon atoms in the considered unit cell, respectively. We obtained the value of -6.87 eV/atom for cohesive energy of this compound which denotes to its a good structural stability. The bond nature for B-C and B-B bonds and bond anisotropy for boron atoms exert B_2C monolayer to reconstruct in a buckled structure.
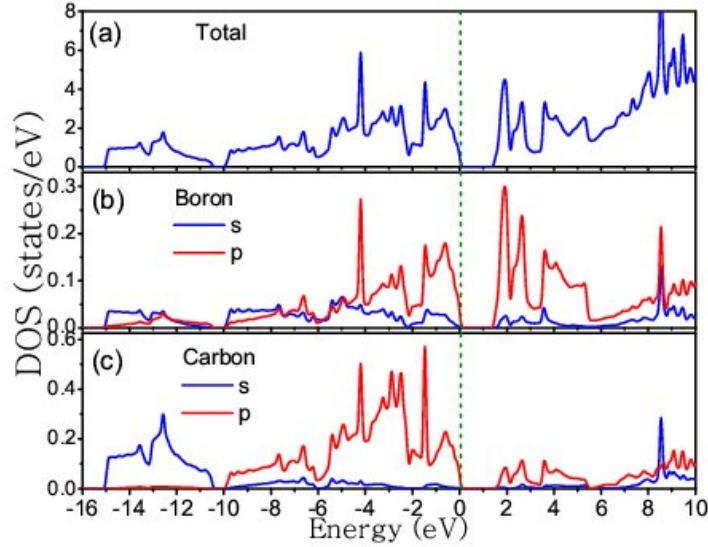
Fig. 2.   The total DOS. (b)The partial DOS for Boron atom. (c)The partial DOS for Carbon atom.

3. Electronic properties

To understand the bond nature of B-C in pentagonal B_2C monolayer , the two-dimensional charge distribution in B-C bond plane is plotted (see Fig.1c). As can be seen from this figure, the charge accumulation around carbon atom is more

remarkable than boron atom. which attributed to due to the electronegativity differences between C and B atoms. Thus, we can claim an ionic-covalent nature for chemical bonding in this compound. This charge distribution expresses that the charge transfer occurs from boron to carbon atoms as this charge transfer process is accomplished. As a result the valence orbitals of both atoms are fully occupied. To gain deep insight into the electronic properties of B_2C, the total and partial density of states (DOS) are plotted in figure 2. The electronic results show that B_2C monolayer in pentagonal structure has semiconducting behavior as there is an energy gap about 1.5 eV in contrast to suggested metallic phase of B_2C monolayer by Shahrokhi et al. [18]. In the monolayer structure which was suggested by Shahrokhi et al., similar to this pentagonal structure, each carbon atom has four boron neighbors and each boron is bond with two carbon and one boron atom. In their presented structure, we can see hexagonal faces, and all B-B bonds are parallel with each others. However, in our structure, there are only pentagonal faces and all B-B bonds are perpendicular with each other. This structural reconstruction leads to full charge transferring process and as a result we can observe semiconduction properties in this structure.

The partial DOS for boron atom illustrates that the s and p orbitals are hybridized with each other and contribute in forming the bonds (see Fig.2b). The p orbital contributes in forming the bond with carbon atoms and s orbital approximately is localized in low energy ranges about -15 to -11 eV (see Fig.2c). The p sub-orbital density of states for boron illustrates that bonding and antibonding orbitals for this atom are related to p_x and p_y sub-orbitals, but p_z sub-orbital plays non-bonding states in density of states and is located in low energy ranges with respect to p_x and p_y sub-orbitals in valence bands (see Fig.3a). On the other hand, p sub-orbitals of carbon atoms have a different arrangement in energy levels in comparison with boron atom(see Fig.3b). The results exhibit that bonding states of carbon, $p_x + p_y$ states, are more stable than non-bonding p_z states.

4. Optical properties

The electronic band structure result exhibits that B_2C monolayer has an indirect band gap (X-Γ) direction. We determined each energy level with a specific color and number to investigate the optical interband transitions. The hybridized orbitals have different proportion in energy levels. The Joint density of states in both directions is plotted to study optical interband transitions. This graph explains the interband transitions from occupied states to unoccupied energy levels.

We determined the main peaks in each direction which exhibited that each peak is related to a transition from an occupied states to an unoccupied state. The first peak in x direction is related to transitions from the highest valence band (5 and 6 levels) to lowest conduction band (7 and 8 levels). These energy levels have similar degeneracy in high symmetry pints, R, Γ, X and M, so we can see a sharp peaks due to transitions from these energy levels. While for the second peak in x direction, we

6   *M. Naseri, et al.,*
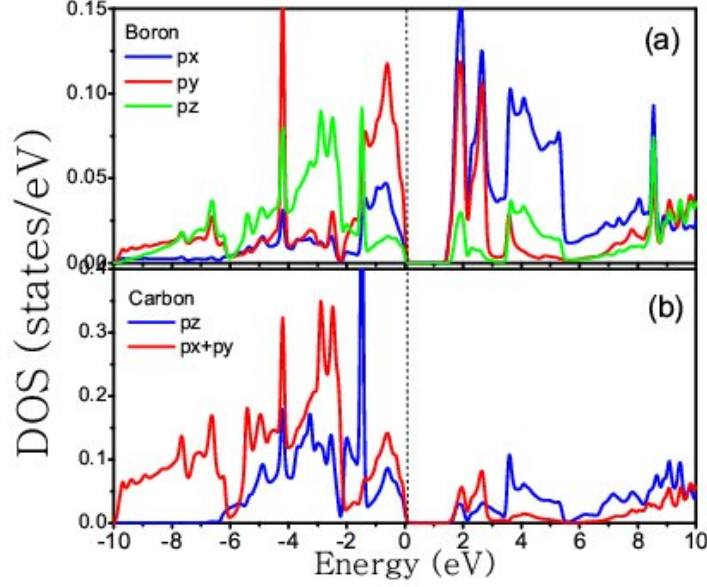
Fig. 3.   (a)The density of states for Boron's sub-orbitals. (b)The density of states for Carbons's sub-orbitals.

can see a broadened shape as this peak is related to transitions from a wide range of valence energy levels to unoccupied conduction levels. The threshold of joint DOS demonstrates optical gap in each direction. The obtained values for this parameters is 2.08 eV for both direction while the energy band gap in band structure was 1.5 eV. This difference exhibits that the first optical transition do not occur from the edge of valence band maximum to conduction band minimum.

Studying optical properties of materials helps to propose various optoelectronic applications. One of the best approaches to start is the calculation of complex dielectric function which seen as a practical tool to identify all optical aspects such as reflectivity percentage as well as absorption spectrum. The complex dielectric function is made up of two contributions; real part and imaginary part, which are related to the following equation:

$$\varepsilon_{complex} = \Re\varepsilon + i\Im\varepsilon \quad , \tag{3}$$

These parts have been identified through equation 2 that takes interband optical transitions between occupied (ik) and unoccupied electron states (fk) [25] into acount.

$$\Im\varepsilon^{\alpha\alpha}(\omega) = \frac{4\pi e^2}{m^2\omega^2} \sum_{i,f} \int \frac{2dk^3}{(2\pi)^3} \big|\langle ik|P_\alpha|fk\rangle\big|^2 f_i^k(1-f_f^k)\delta(E_f^k - E_i^k - \hbar\omega) \quad , \tag{4}$$
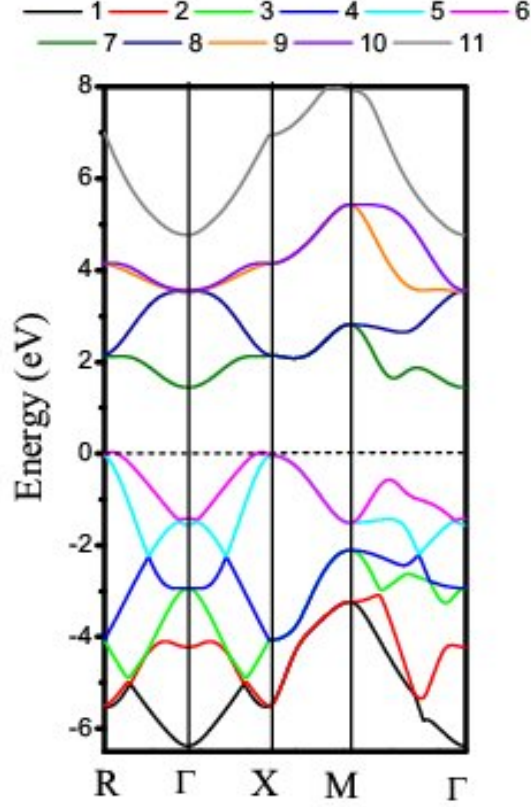
Fig. 4. The orbital contributions in energy band structure are determined to investigate the energy levels.

On the other hand, Kramers-Kronig relations define a relationship between imaginary and real parts of this function. The real part of the dielectric function is obtained correspondingly:

$$\Re\varepsilon^{\alpha\beta}(\omega) = \delta_{\alpha\beta} + \frac{2}{\pi}Pr.\int_0^\infty \frac{\Im\varepsilon^{\alpha\beta}(\omega^{'})}{\omega^{'2} - \omega^2}\omega^{'}d\omega^{'} \quad . \tag{5}$$

Where Pr. denotes to the Cauchy principal value. In this section, two important optical spectra have been discussed: optical absorption and reflectivity spectrum. The reflectivity spectrum of B_2C monolayer displays a transparent behavior in the visible range of the light in z direction (see Fig.6a). For the investigated compound this parameter is about %2.5 , but in x direction, we can see a different manner. There are some remarkable regions in reflectivity spectrum in x direction. The first region is wider than the other which is situated between 2-4 eV and the second region is broadened around 4-7 eV. The third one is in 10-16 eV. These regions

8   *M. Naseri, et al.,*
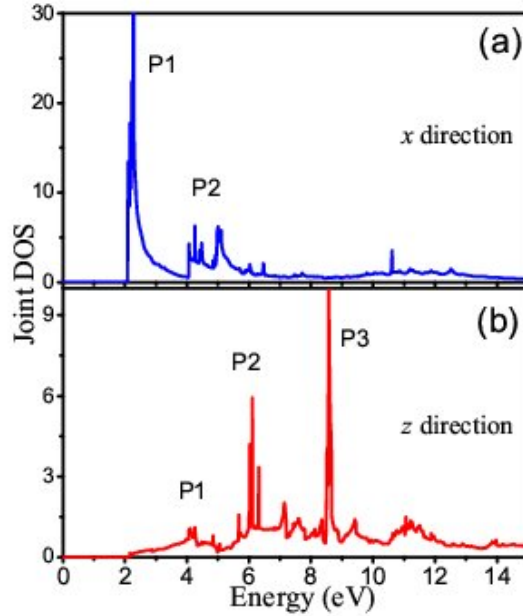
Fig. 5.   The joint density of states for optical interband transitions in (a) x and (b) z directions.

in reflectivity spectrum are due to collective exciations. The first and second peaks that are more noteworthy than the third peak are due to π electrons that are excited by incident photon. The third peak is related to $\pi + \sigma$ collective exciations. In these regions the incident photons have the highest interaction with the compound, so a notable reflectivity is observed . Also, this spectrum in both directions decreases to neglectable value by increasing incident photon energy.

The other important optical spectrum is absorption that defines the exciations of valence electrons by photons and transfer them to unoccupied conduction band. Optical absorption for B_2C monolayer is illustrated in Fig.6b. There are a series of peaks are seen in this spectrum in both directions. The sharp peaks are attributed to the fact that the optical transition from the degenerate and thin energy levels to conduction band. The optical transitions from broadened energy levels in valence band leads to emergence of the broaded peaks in optical absorption spectrum. For x direction, we can see more sharper peaks in low energy ranges with respect to z direction. As seen in joint DOS, these peaks were due to degenerated energy levels in the edge of valence conduction band. Also, the results demonstrate a suitable absorption value in the visible range of light that persuade us to design solar cell devices through this monolayer nanostructure.
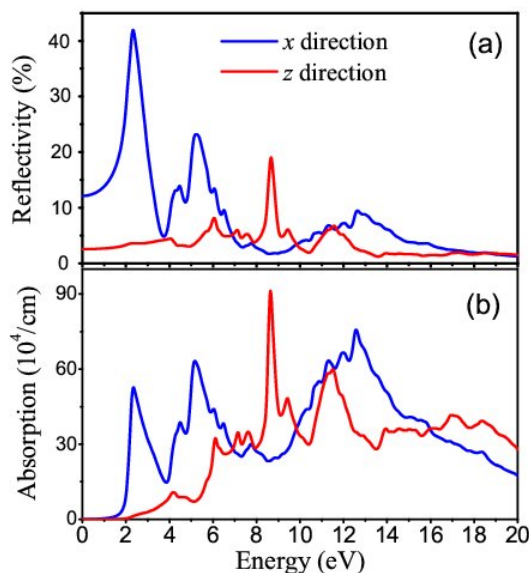
Fig. 6. (a)The reflectivity spectrum of B_2C monolayer. (b) The absorption spectrum of B_2C monolayer.

5. Conclusions

In summary, the electronic and optical properties of pentagonal face B_2C have been investigated by the fist principles calculations. The structural results, cohesive energy of system, exhibit that this monolayer has a good structural stability and its possible to synthesize it in equilibrium conditions in laboratory. Also, we saw an indirect energy band gap in electronic band structure about 1.5 eV that make it a good candidate for optoelectronic devices. The optical calculations for B_2C were more attractive because it has a low percentage of reflectivity spectrum in visible range, about %2.5. On the other hand, the optical absorption in visible range of light persuade us to design new types of two-dimensional nano-base solar cell.

Acknowledgements

1. Y. Peng, Y. Li, Y. Ban, H. Jin, W. Jiao, X. Liu, W. Yang, Metal-Organic Framework Nanosheets as Build- ing Blocks for Molecular Sieving Membranes, Science. 346 (2014) 1356-1359.
2. T. Rodenas, I. Luz, G. Prieto, B. Seoane, H. Miro, A. Corma, F. Kapteijn, L. Xamena, J. Gascon, Metal-Organic Framework Nanosheets in Polymer CompositeMaterials for Gas Separation, Nat. Mater. 14 (2015) 48-55.
3. J.W. Colson, A.R. Woll, A. Mukherjee, M.P. Levendorf, E.L. Spitler, V.B. Shields, M.G. Spencer, J. Park, W.R. Dichtel, Oriented 2D Covalent Organic Framework Thin Films on Single-Layer Graphene, Science. 332 (2011) 228-231.
4. M.J. Kory, M. Wörle, T. Weber, P. Payamyar, S.W. van de Poll, J. Dshemuchadse, N. Trapp, A.D. Schlüter, Gram-Scale Synthesis of Two-Dimensional Polymer Crystals and Their Structure Analysis by X-Ray Diffraction, Nat. Chem. 6 (2014) 779-784.
5. P. Kissel, D.J. Murray, W.J. Wulftange, V.J. Catalano, B.T. King, A Nanoporous Two-Dimensional Polymer by Single-Crystal-to-Single-Crystal Photopolymerization, Nat. Chem. 6 (2014) 774-778.
6. C.L. Tan, X.Y. Qi, X. Huang, J. Yang, B. Zheng, Z.F. An, R.F. Chen, J. Wei, B.Z. Tang, W. Huang, H. Zhang, Single-Layer Transition Metal Dichalcogenide Nanosheet-Assisted Assembly of Aggregation-Induced Emission Molecules to Form Organic Nanosheets with Enhanced Fluorescence, Adv. Mater. 26 (2014) 1735-1739.
7. H. Liu, Y. Du, Y. Deng, P.D. Ye, Semiconducting Black Phosphorus: Synthesis, Transport Properties and Electronic Applications, Chem. Soc. Rev. 44 (2015) 2732-2743.
8. B. Lalmi, H. Oughaddou, H. Enriquez, A. Kara, S. Vizzini, B. Ealet, B. Aufray, Epitaxial Growth of a Silicene Sheet, Appl. Phys. Lett. 97 (2010) 223109.
9. A. Fathalian, J. Jalilian, First principle study of unzipped zinc oxide nanotubes, Phys. Lett. A. 374 (2010) 4695-4699.
10. J. Qiu, M. Guo, X. Wang, Electrodeposition of Hierarchical ZnO Nanorod-Nanosheet Structures and Their Applications in Dye-Sensitized Solar Cells, ACS Appl. Mater. Interfaces. 3 (2011) 2358-2367.
11. M. Naguib, V.N. Mochalin, M.W. Barsoum, Y. Gogotsi, 25th Anniversary Article: MXenes: A New Family of Two-Dimensional Materials, Adv. Mater. 26 (2014) 992-1005.
12. N. Wang, Y. Tian, J. Zhao, P. Jin, CO oxidation catalyzed by silicon carbide (SiC) monolayer: A theoretical study, J. Molec. Graph. Modell. 66 (2016) 196200.
13. H.H. Nersisyan, B.U. Yoo, S.H. Joo, T.H. Lee, K.-H. Lee, J.-H. Lee, Polymer assisted approach to two-dimensional (2D) nanosheets of B_4C, Chem. Eng. J. 281 (2015) 218-226.
14. H. Jeong et al. SemiconductorInsulatorSemiconductor Diode Consisting of Monolayer MoS2, h-BN, and GaN Heterostructure, ACS Nano. 9 (2015) 10032-10038.
15. J. Jalilian, M. Safari, Tuning of the electronic and optical properties of single-layer boron nitride by strain and stress, Diamond. Rela. Mater. 66 (2016) 163-170.
16. A. Gupta, T. Sakthivela, S. Seal, Recent development in 2D materials beyond graphene, Prog. Mater. Sci. 73 (2015) 44126.
17. X. Wu, Y. Pei, Z. Cheng, B_2C Graphene, Nanotubes, and Nanoribbons, Nano Lett. 9 (2009) 1577-1582.
18. M. Shahrokhi, S. Naderi, A. Fathalian, Ab initio calculations of optical properties of

B2C graphene sheet, Solid. State. Comm. 152 (2012) 1012-1017.

19. F. Li, K. Tu, H. Zhang, Ch. Chen, Flexible structural and electronic properties of a pentagonal B_2C monolayer via external strain: a computational investigation, Phys. Chem. Chem. Phys. 17 (2015) 24151-24156.
20. P. Blaha, K. Schwarz, G.K.H. Madsen, D. Kvasnicka, J. Luitz, K. Schwarz, An augmented PlaneWave+Local Orbitals Program for calculating crystal properties revised edition WIEN2k 13.1 (release 06/26/2013) Wien2K users guide, ISBN 3-9501031-1-2.
21. J.P. Perdew, K. Burke, M. Ernzerhof, Generalized Gradient Approximation Made Simple, Phys. Rev. Lett. 77 (1996) 3865-3868
22. H.J. Monkhorst, J.D. Pack, Special points for Brillouin-zone integrations, Phys. Rev. B 13 (1995) 5188.
23. H. Ehrenreich, M.H. Cohen, Self-Consistent Field Approach to the Many-Electron Problem, Phys. Rev. 115 (1959) 786-790.
24. F. Birch, Equation of state and thermodynamic parameters of NaCl to 300 kbar in the high-temperature domain, J. Geophys. Res. B 83 (1978) 1257-1268
25. R. Abt, C. Ambrosch-Draxl, P. Knoll, Optical response of high temperature superconductors by full potential LAPW band structure calculations, Phys. B: Cond. Matt. 194196 (1994) 1451-1452.